Inducing a Magnetic Monopole with Topological Surface States

Xiao-Liang Qi,[1] Rundong Li,[1] Jiadong Zang,[2] Shou-Cheng Zhang[1]*

Existence of the magnetic monopole is compatible with the fundamental laws of nature; however, this elusive particle has yet to be detected experimentally. We show theoretically that an electric charge near a topological surface state induces an image magnetic monopole charge due to the topological magneto-electric effect. The magnetic field generated by the image magnetic monopole may be experimentally measured, and the inverse square law of the field dependence can be determined quantitatively. We propose that this effect can be used to experimentally realize a gas of quantum particles carrying fractional statistics, consisting of the bound states of the electric charge and the image magnetic monopole charge.

The electromagnetic response of a conventional insulator is described by a dielectric constant ε and a magnetic permeability μ. An electric field induces an electric polarization, whereas a magnetic field induces a magnetic polarization. As both the electric field $\mathbf{E}(x)$ and the magnetic induction $\mathbf{B}(x)$ are well defined inside an insulator, the linear response of a conventional insulator can be fully described by the effective action $S_0 = \frac{1}{8\pi}\int d^3x dt\left(\varepsilon\mathbf{E}^2 - \frac{1}{\mu}\mathbf{B}^2\right)$, where d^3xdt is the volume element of space and time. However, in general, another possible term is allowed in the effective action, which is quadratic in the electromagnetic field, contains the same number of derivatives of the electromagnetic potential, and is rotationally invariant; this term is given by $S_\theta = \left(\frac{\theta}{2\pi}\right)\left(\frac{\alpha}{2\pi}\right)\int d^3x dt \mathbf{E}\cdot\mathbf{B}$. Here, $\alpha = \frac{e^2}{\hbar c}$ (where $\hbar$ is Planck's constant h divided by 2π and c is the speed of light) is the fine-structure constant, and θ can be viewed as a phenomenological parameter in the sense of the effective Landau-Ginzburg theory. This term describes the magneto-electric effect (*1*), where an electric field can induce a magnetic polarization, and a magnetic field can induce an electric polarization.

Unlike conventional terms in the Landau-Ginzburg effective actions, the integrand in S_θ is a total derivative term, when $\mathbf{E}(x)$ and $\mathbf{B}(x)$ are expressed in terms of the electromagnetic vector potential (where ∂^μ denotes the partial derivative; μ, ν, ρ, and τ denote the spacetime coordinates; $F^{\mu\nu}$ is the electromagnetic field tensor; and A^μ is the electromagnetic potential)

$$S_\theta = \frac{\theta}{2\pi}\frac{\alpha}{16\pi}\int d^3x dt \varepsilon_{\mu\nu\rho\tau}F^{\mu\nu}F^{\rho\tau} = \frac{\theta}{2\pi}\frac{\alpha}{4\pi}\int d^3x dt \partial^\mu(\varepsilon_{\mu\nu\rho\sigma}A^\nu\partial^\rho A^\tau) \quad (1)$$

Furthermore, when a periodic boundary condition is imposed in both the spatial and temporal directions, the integral of such a total derivative term is always quantized to be an integer; i.e., $\frac{S_\theta}{h} = \theta n$ (where n is an integer). Therefore, the partition function and all physically measurable quantities are invariant when the θ parameter is shifted by 2π times an integer (*2*). Under time-reversal symmetry, $e^{i\theta n}$ is transformed into $e^{-i\theta n}$ (here, $i^2 = -1$). Therefore, all time-reversal invariant insulators fall into two general classes, described by either $\theta = 0$ or $\theta = \pi$ (*3*). These two time-reversal invariant classes are disconnected, and they can only be connected continuously by time-reversal breaking perturbations. This classification of time-reversal invariant insulators in terms of the two possible values of the θ parameter is generally valid for insulators with arbitrary interactions (*3*). The effective action contains the complete description of the electromagnetic response of topological insulators. Topological insulators have an energy gap in the bulk, but gapless surface states protected by the time-reversal symmetry. We have shown (*3*) that such a general definition of a topological insulator reduces to the Z_2 topological insulators described in (*4*–*6*) for non-interacting band insulators; this finding is a three-dimensional (3D) generalization of the quantum spin Hall insulator in two dimensions (*7*–*10*). For generic band insulators, the parameter θ has a microscopic expression of the momentum space Chern-Simons form (*3*, *11*). Recently, experimental evidence of the topologically nontrivial surface states has been observed in $Bi_{1-x}Sb_x$ alloy (*12*), which supports the theoretical prediction that $Bi_{1-x}Sb_x$ is a Z_2 topological insulator (*4*).

With periodic temporal and spatial boundary conditions, the partition function is periodic in θ under the 2π shift, and the system is invariant under the time-reversal symmetry at $\theta = 0$ and $\theta = \pi$. However, with open boundary conditions, the partition function is no longer periodic in θ, and time-reversal symmetry is generally broken (but only on the boundary), even when $\theta = (2n + 1)\pi$. Our work in (*3*) gives the following physical interpretation: Time-reversal invariant topological insulators have a bulk energy gap but have gapless excitations with an odd number of Dirac cones on the surface. When the surface is coated with a thin magnetic film, time-reversal symmetry is broken, and an energy gap also opens up at the surface. In this case, the low-energy theory is completely determined by the surface term in Eq. 1. As the surface term is a Chern-Simons term, it describes the quantum Hall effect on the surface. From the general Chern-Simons-Landau-Ginzburg theory of the quantum Hall effect (*13*), we know that the coefficient $\theta = (2n+1)\pi$ gives a quantized Hall conductance of $\sigma_{xy} = \left(n + \frac{1}{2}\right)\frac{e^2}{h}$. This quantized Hall effect on the surface is the physical origin behind the topological magneto-electric (TME) effect. Under an applied electric field, a quantized Hall current is induced on the surface, which in turn generates a magnetic polarization and vice versa.

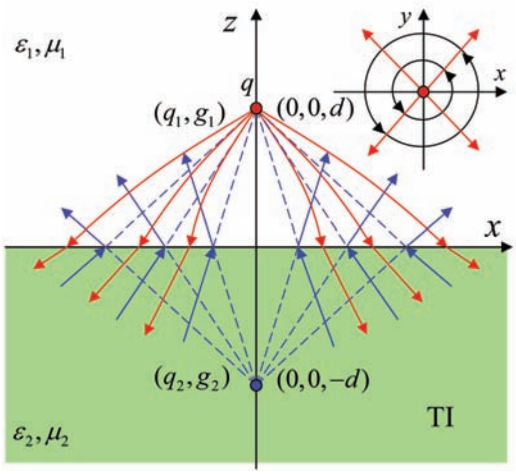

Fig. 1. Illustration of the image charge and monopole of a point-like electric charge. The lower-half space is occupied by a topological insulator (TI) with dielectric constant ε_2 and magnetic permeability μ_2. The upper-half space is occupied by a topologically trivial insulator (or vacuum) with dielectric constant ε_1 and magnetic permeability μ_1. A point electric charge q is located at (0, 0, d). When seen from the lower-half space, the image electric charge q_1 and magnetic monopole g_1 are at (0, 0, d); when seen from the upper-half space, the image electric charge q_2 and magnetic monopole g_2 are at (0, 0, $-d$). The red solid lines represent the electric field lines, and blue solid lines represent magnetic field lines. (Inset) Top-down view showing the in-plane component of the electric field at the surface (red arrows) and the circulating surface current (black circles).

[1]Department of Physics, Stanford University, Stanford, CA 94305–4045, USA. [2]Department of Physics, Fudan University, Shanghai, 200433, China.

*To whom correspondence should be addressed. E-mail: sczhang@stanford.edu

We propose a manifestation of the TME effect. When a charged particle is brought close to the surface of a topological insulator, a magnetic monopole charge is induced as a mirror image of the electric charge. The full set of electromagnetic field equations can be obtained from the functional variation of the action $S_0 + S_\theta$ (*14*), and they can be presented as conventional Maxwell's equations but with the modified constituent equations describing the TME effect (*3*)

$$\begin{aligned}\mathbf{D} &= \mathbf{E} + 4\pi\mathbf{P} - 2\alpha P_3\mathbf{B}\\ \mathbf{H} &= \mathbf{B} - 4\pi\mathbf{M} + 2\alpha P_3\mathbf{E}\end{aligned} \qquad (2)$$

where $P_3(x) = \theta(x)/2\pi$ is the magneto-electric polarization (*3*), **D** is the electric displacement, **P** is the electric polarization, **H** is the magnetic field, and **M** is the magnetization. It takes the value of $P_3 = 0$ in vacuum or conventional insulators and $P_3 = \pm1/2$ in topological insulators, with the sign determined by the direction of the surface magnetization.

Now consider the geometry as shown in Fig. 1. The lower-half space ($z < 0$) is occupied by a topological insulator with a dielectric constant ε_2 and a magnetic permeability μ_2, whereas the upper-half space ($z > 0$) is occupied by a conventional insulator with a dielectric constant ε_1 and a magnetic permeability μ_1. A point electric charge q is located at $(0, 0, d)$ with $d > 0$. The Maxwell equations, along with the modified constituent equations and the standard boundary conditions, constitute a complete boundary value problem. To solve this problem, the method of images (*15*) can be used. We assume that, in the lower-half space, the electric field is given by an effective point charge q/ε_1 and an image charge q_1 at $(0, 0, d)$, whereas the magnetic field is given by an image magnetic monopole g_1 at $(0, 0, d)$. In the upper-half space, the electric field is given by q/ε_1 at $(0, 0, d)$ and an image charge q_2 at $(0, 0, -d)$; the magnetic field is given by an image magnetic monopole g_2 at $(0, 0, -d)$. The above ansatz satisfies the Maxwell equations on each side of the boundary. At the boundary $z = 0$, the solution is then matched according to the standard boundary condition, giving

$$\begin{aligned} q_1 &= q_2\\ &= \frac{1}{\varepsilon_1}\frac{(\varepsilon_1-\varepsilon_2)(1/\mu_1+1/\mu_2)-4\alpha^2P_3^2}{(\varepsilon_1+\varepsilon_2)(1/\mu_1+1/\mu_2)+4\alpha^2P_3^2}q\\ g_1 &= -g_2\\ &= -\frac{4\alpha P_3}{(\varepsilon_1+\varepsilon_2)(1/\mu_1+1/\mu_2)+4\alpha^2P_3^2}q \end{aligned} \qquad (3)$$

We will first take $\varepsilon_1 = \varepsilon_2 = \mu_1 = \mu_2 = 1$ below and then recover the $\varepsilon_{1,2}$, $\mu_{1,2}$ when discussing the experimental proposals later. The solution shows that, for an electric charge near the surface of a topological insulator, both an image magnetic monopole and an image electric charge will be induced, as compared with conventional electromagnetic media where only an electric image charge will be induced. It is notable that the magnitudes of the image magnetic monopole and image electric charge satisfy the relation $q_{1,2} = \pm(\alpha P_3)g_{1,2}$. This is just the relation $q = (\theta/2\pi)g$ for the electric and magnetic charges of a dyon inside the θ vacuum (*16*), with $\theta/2\pi = \pm P_3$ here.

The physical origin of the image magnetic monopole is understood by rewriting part of the Maxwell equations as

$$\nabla \times \mathbf{B} = 2\alpha P_3\delta(z)\hat{\mathbf{n}} \times \mathbf{E} \qquad (4)$$

with $P_3 = \pm1/2$ the value for the topological insulator [in the above equation, ∇ is the derivative vector, $\hat{\mathbf{n}}$ is the normal vector of the surface, and $\delta(z)$ is the Dirac δ function]. The right-hand side of the above equation corresponds to a surface current density $\mathbf{j} = \sigma_{xy}(\hat{\mathbf{n}} \times \mathbf{E})$, which is induced by the in-plane component of the electric field and is perpendicular to this component. This current is nothing but the quantized Hall current mentioned earlier. For the problem under consideration, the surface current density is calculated as

$$\mathbf{j} = P_3\left(\frac{e^2}{h}\right)\left(\frac{q}{1+\alpha^2P_3^2}\right)\frac{r}{(r^2+d^2)^{\frac{3}{2}}}\hat{\mathbf{e}}_\varphi \qquad (5)$$

which is circulating around the origin (inset of Fig. 1) (here, r is the radial distance and $\hat{\mathbf{e}}_\varphi$ is the tangential unit vector). Physically, this surface current is the source that induces the magnetic field. On each side of the surface, the magnetic field induced by the surface current can be viewed as the field induced by an image magnetic monopole on the opposite side.

According to the above calculation, the image magnetic monopole field indeed has the correct magnetic field dependence expected from a monopole, and it can be controlled completely through the position of the electric charge. As we started with the Maxwell's equation, which includes $\nabla \cdot \mathbf{B} = 0$, the magnetic flux integrated over a closed surface must vanish. We can check that this is the case by considering a closed surface—for example, a sphere with radius a—that encloses a topological insulator. The detailed calculation is presented in the supporting online material (*17*). Inside the closed surface, there is not only a image magnetic monopole charge, but also a line of magnetic charge density whose integral exactly cancels the point image magnetic monopole. However, when the separation between the electric charge and the surface (d) is much smaller than the spherical radius (a), the magnetic field is completely dominated by the image magnetic monopole, and the contribution due to the line of magnetic charge density is vanishingly small. Therefore, we propose here to experimentally observe the magnetic monopole in the same sense that we can experimentally observe other fractionalization, or de-confinement, phenomena in condensed matter physics. In any closed electronic system, the total charge must be quantized to be an integer. However, one can separate fractionally charged elementary

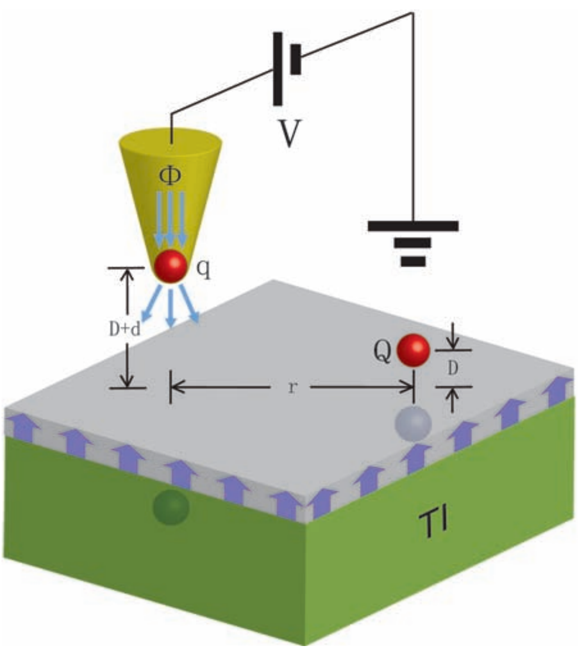

Fig. 2. Illustration of the experimental setup to measure the image monopole. A magnetic layer is deposited on the surface of the topological insulator, as indicated by the layer with blue arrows. (The same layer is drawn in Figs. 3 and 4.) A scanning MFM tip carries a magnetic flux ϕ and a charge q. A charged impurity is confined on the surface with charge Q and distance D out of the surface. By scanning over the voltage V and the distance r to the impurity, the effect of the image monopole magnetic field can be measured (see text).

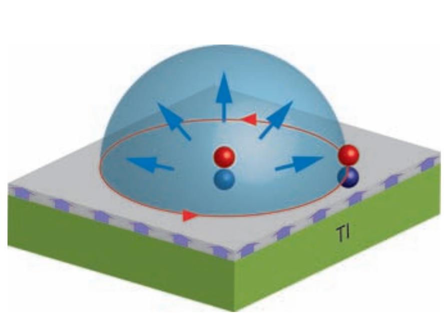

Fig. 3. Illustration of the fractional statistics induced by image monopole effect. Each electron forms a dyon with its image monopole. When two electrons are exchanged, an AB phase factor is obtained (which is determined by half of the image monopole flux) and leads to statistical transmutation.

excitations arbitrarily far from each other, so that fractional charge can have well-defined meaning locally. A similar situation occurs in spin-charge separation. Whereas the total charge and the total spin of a closed system must be linked to each other, spin and charge can occur as separated local excitations. In our case, as long as d is much smaller than the radius of curvature of a topological surface a, the local magnetic field is completely determined by a single image magnetic monopole.

Such an image monopole can be observed experimentally by a magnetic force microscope (MFM). Consider the surface of the topological insulator with a localized charged impurity (Fig. 2). A scanning MFM tip can be applied to detect the magnetic field distribution of the image monopole. However, the charge of the impurity also generates an electric force to the tip. The contribution of the image monopole can be distinguished from other trivial contributions by scanning both the tip position r and the tip voltage V. For a given position r, $f_{\min}(r)$ defines the minimal force applied to the tip when scanning the voltage, and D is the distance of the charged impurity to the surface. In the limit of $r >> D$, the conventional charge interaction leads to a $1/r^6$ dependence of $f_{\min}(r)$. The image monopole magnetic field leads to more dominant contribution

$$f_{\min}(r) \simeq \frac{4\alpha P_3}{(1+\varepsilon_2/\varepsilon_1)(1/\mu_1+1/\mu_2)-4\alpha^2 P_3^2}\frac{Q\phi}{r^3} \tag{6}$$

in which Q is the impurity charge and ϕ is the net flux of the magnetic tip. For the estimated parameters $\varepsilon_2 \cong 100$ for the $Bi_{1-x}Sb_x$ alloy (*18*), $\varepsilon_1 = 1$, $\mu_1 \cong \mu_2 \cong 1$, $\phi \cong 2.5hc/e$, and a typical distance $r = 50$ nm, the force is $f_{\min}(r) \cong 0.3$ pN/μm, which is observable in the present experiments. In a real experimental system, the surface magnetic layer can have defects such as domains and steps that induce an inhomogeneous fringe magnetic field acting on the MFM tip. However, all surface roughness effects can only induce magnetic field of dipolar or higher order. Consequently, the contribution of surface roughness decays faster than $1/r^3$ so that the monopole contribution proportional to $1/r^3$ still dominates the long-range behavior. Further detail on the calculations is presented in the supporting online material (*17*).

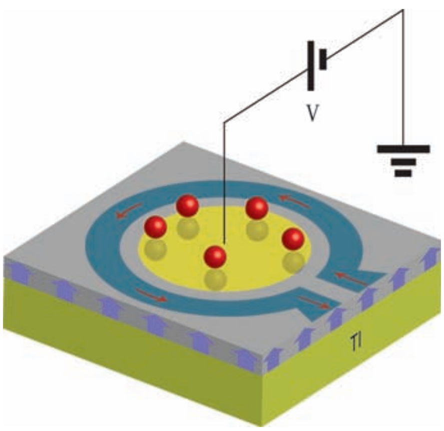

Fig. 4. Illustration of the experimental proposal measuring the fractional statistics of the dyons. When a gate voltage is applied to the central metallic island, the number of electrons in the central island can be tuned, which in turn changes the net flux threaded in the superconducting ring and leads to a supercurrent.

Because the position of the image monopole is determined by that of the charge above the surface, the pure monopole is not an elementary excitation of the system, and this is different from the monopole proposed in some spin ice models (*19*). However, if we consider the electrons moving on the topological surface as part of the system, the bound state of an electron and its image monopole does become a dynamical object with nontrivial properties. Such a bound state of charge and monopole is known in high-energy physics as a "dyon" (*16*)": a composite particle with both electric and magnetic charges. Besides contributing a monopole-monopole Coulomb interaction, the image monopole also induces a statistical interaction between two dyons. When two dyons are exchanged, each of them will obtain an Aharonov-Bohm (AB) phase due to the magnetic field of the other one. The net AB phase obtained by the two-particle system during an exchange process is independent of the path of the particles on the 2D plane, which thus can be interpreted as a statistical angle of the dyon (Fig. 3). Therefore, this setup provides a condensed matter realization of the anyon concept (*20*, *21*) in the absence of any external magnetic field. Anyons have unusual quantum statistics; interchanging a pair of them gives rise to a complex phase factor different from zero (as in the case of bosons) or π (as in the case of fermions). This effect also provides a mechanism of statistical transmutation in (3+1) dimensions (*22*, *23*). If each dyon has charge q and monopole flux g, then the statistical angle is given by $\varphi = \left(\frac{gq}{2\hbar c}\right)$. For example, the binding of an electron with charge e and a monopole with flux hc/e leads to $\varphi = \pi$, in which case the dyon is a boson. However, there is a difference between the dyon studied here and that in high-energy physics. In high-energy physics, the charged particle and monopole are point-like particles moving in three dimensions. Consequently, the monopole flux must be quantized in unit of hc/e, and correspondingly, the statistical angle φ can only be 0 or π modular 2π. This is consistent with the fact that there are no anyonic statistics in (3+1) dimensions. Our dyon can only be defined if an electron is moving close to the surface of a topological insulator. Consequently, the dyon is always confined to a 2D surface. In this case, $\nabla \cdot \mathbf{B} = 0$ is satisfied everywhere and the flux of the image monopole does not have to be quantized. Correspondingly, the dyon can have anyonic statistics. [A possibly related anyon model has been studied in the fractional quantum Hall context (*24*).] According to Eq. 3, the statistical angle of an electron-induced dyon is

$$\varphi = \frac{2\alpha^2 P_3}{(\varepsilon_1+\varepsilon_2)(1/\mu_1+1/\mu_2)+4\alpha^2 P_3^2} \tag{7}$$

which is of order α^2 and can generally be irrational (*25*). It should be noticed that the image charge beneath the electron does not contribute additional AB phase because its motion corresponds to a displacement current. For $P_3 = 1/2$ and $\varepsilon_1, \mu_1, \mu_2 \sim 1$, $\varepsilon_2 \sim 100$, we obtain $\varphi \cong \alpha^2/200 \cong 2.6 \times 10^{-7}$ rad. Though the statistical angle is quite small, it is physically observable. With the geometry of Fig. 4, a quasi-1D superconducting ring and a metallic island surrounded by the ring are deposited on top of the topological insulator surface (which has already been gapped by a magnetic layer). By tuning the gate voltage of the central island, the number of electrons N on the island can be tuned. Because of the statistical angle φ given by Eq. 7, each electron in the central island induces a flux of φ seen by the electrons in the ring. Consequently, the net flux through the ring is $N\varphi$ in unit of the flux quanta, which generates a supercurrent in the superconducting ring as in a standard superconducting quantum interference device. For a typical electron density of $n = 10^{11}/\mathrm{cm}^2$ and island size $R = 1$ μm, the net magnetic flux is $n\varphi\pi R^2\hbar c/e \simeq 2.6 \times 10^{-4} hc/2e$, and the corresponding magnetic field is $B = n\varphi\hbar c/e \simeq 1.7 \times 10^{-3}$G, which is observable. It is possible to have some other topological insulator material with a smaller dielectric constant ε_2, in which the statistical angle of the dyon can be larger.

We have shown theoretically that the topological surface states of a 3D topological insulator can act as a mirror that images an electron as a magnetic monopole. Such a transmutation between electric field and magnetic field is a direct manifestation of the TME effect (*3*). Because of this effect, a 2D electron gas in the neighborhood of the surface will become a dyon gas with fractional statistics. We have presented realistic experimental setups to observe the field of the image magnetic monopole and the statistical angle of the dyon.

References and Notes

1. L. D. Landau, E. M. Lifshitz, *Electrodynamics of Continuous Media* (Pergamon, Oxford, 1984).
2. E. Witten, *Sel. Math. New Ser.* **1**, 383 (1995).
3. X.-L. Qi, T. L. Hughes, S.-C. Zhang, *Phys. Rev. B* **78**, 195424 (2008).
4. L. Fu, C. L. Kane, *Phys. Rev. B* **74**, 195312 (2006).
5. J. E. Moore, L. Balents, *Phys. Rev. B* **75**, 121306 (2007).
6. R. Roy, preprint available at http://arxiv.org/abs/cond-mat/0604211.
7. C. L. Kane, E. J. Mele, *Phys. Rev. Lett.* **95**, 226801 (2005).
8. B. A. Bernevig, S.-C. Zhang, *Phys. Rev. Lett.* **96**, 106802 (2006).
9. B. A. Bernevig, T. L. Hughes, S.-C. Zhang, *Science* **314**, 1757 (2006).
10. M. König *et al.*, *Science* **318**, 766 (2007); published online 19 September 2007 (10.1126/science.1148047).
11. A. M. Essin, J. E. Moore, D. Vanderbilt, preprint availble at http://arxiv.org/abs/0810.2998.

12. D. Hsieh *et al.*, *Nature* **452**, 970 (2008).
13. S.-C. Zhang, T. H. Hansson, S. Kivelson, *Phys. Rev. Lett.* **62**, 82 (1989).
14. F. Wilczek, *Phys. Rev. Lett.* **58**, 1799 (1987).
15. J. D. Jackson, *Classical Electrodynamics* (Wiley, New York, 1999).
16. E. Witten, *Phys. Lett. B* **86**, 283 (1979).
17. See supporting material on *Science* Online.
18. O. Madelung, U. Rössler, M. Schulz, in *Landolt-Börnstein, Substance/Property Index, Semiconductors, Non-Tetrahedrally Bonded Elements and Binary Compounds I, Subvolume III/17E-17F-41C* (Springer, Berlin, 1998), pp. 1–11.
19. C. Castelnovo, R. Moessner, S. L. Sondhi, *Nature* **451**, 42 (2008).
20. J. Leinaas, J. Myrheim, *Nuovo Cim. B* **37**, 1 (1977).
21. F. Wilczek, *Phys. Rev. Lett.* **49**, 957 (1982).
22. R. Jackiw, C. Rebbi, *Phys. Rev. Lett.* **36**, 1116 (1976).
23. P. Hasenfratz, G. 't Hooft, *Phys. Rev. Lett.* **36**, 1119 (1976).
24. E. Fradkin, S. Kivelson, *Nucl. Phys. B* **474**, 543 (1996).
25. C. Chamon *et al.*, *Phys. Rev. Lett.* **100**, 110405 (2008).
26. We thank O. M. Auslaender, T. L. Hughes, S. Kivelson, and L. Luan for insightful discussions. This work is supported by the U.S. Department of Energy, Office of Basic Energy Sciences under contract DE-AC03-76SF00515.

Supporting Online Material
www.sciencemag.org/cgi/content/full/1167747/DC1
SOM Text
Figs. S1 to S5
References

27 October 2008; accepted 16 January 2009
Published online 29 January 2009;
10.1126/science.1167747
Include this information when citing this paper.

Global Cooling During the Eocene-Oligocene Climate Transition

Zhonghui Liu,[1,2]* Mark Pagani,[1]* David Zinniker,[1] Robert DeConto,[3] Matthew Huber,[4] Henk Brinkhuis,[5] Sunita R. Shah,[6] R. Mark Leckie,[3] Ann Pearson[6]

About 34 million years ago, Earth's climate shifted from a relatively ice-free world to one with glacial conditions on Antarctica characterized by substantial ice sheets. How Earth's temperature changed during this climate transition remains poorly understood, and evidence for Northern Hemisphere polar ice is controversial. Here, we report proxy records of sea surface temperatures from multiple ocean localities and show that the high-latitude temperature decrease was substantial and heterogeneous. High-latitude (45 degrees to 70 degrees in both hemispheres) temperatures before the climate transition were ~20°C and cooled an average of ~5°C. Our results, combined with ocean and ice-sheet model simulations and benthic oxygen isotope records, indicate that Northern Hemisphere glaciation was not required to accommodate the magnitude of continental ice growth during this time.

The abrupt shift to glacial conditions near the Eocene-Oligocene (E-O) boundary ~33.7 million years ago (Ma) is characterized by a ~+1.5 per mil (‰) change in oxygen isotopic ($\delta^{18}O$) values of benthic foraminifera (*1*–*3*) in ~300,000 years, which is indicative of continental ice accumulation and high-latitude cooling, and an ~1-km deepening of the global calcite compensation depth (CCD) (*2*). Proposed causes for this fundamental change in Earth's climate state include changes in ocean circulation due to the opening of Southern Ocean gateways (*4*), a decrease in atmospheric CO_2 (*5*–*8*), and a minimum in solar insolation (*2*).

How Earth's temperature changed during ice expansion is poorly defined, largely because benthic $\delta^{18}O$ records do not distinguish between ice volume and temperature. Deep-sea temperature records based on foraminiferal Mg/Ca ratios show little change during ice expansion (*9*–*11*). As a result, benthic $\delta^{18}O$ records imply E-O ice volumes that must be accommodated by Northern Hemisphere glaciation (*2*, *9*, *12*). This conclusion is nearly untenable given scant physical evidence for Northern Hemisphere ice sheets before the latest Miocene (*7*, *12*–*15*). Deep-water foraminiferal Mg/Ca ratios could be affected by factors other than temperature (*9*, *11*), including a deepening of the CCD (*2*) and changes in deep-water carbonate ion concentration that occurred during the E-O climate transition. Indeed, shallow-water Mg/Ca–based temperatures, from exceptionally well-preserved foraminifera deposited above the CCD, indicate ~2.5°C of cooling in the tropics (*14*, *15*) and cast further suspicion on deep-water Mg/Ca–based temperatures across this major CCD deepening event.

Here, we report E-O sea surface temperature (SST) changes, which were determined with alkenone unsaturation index ($U^{K'}_{37}$) and tetraether index (TEX_{86}) (*16*, *17*), from 11 globally dispersed ocean localities. These localities include Ocean Drilling Program/Deep Sea Drilling Project (ODP/DSDP) sites 277, 336, 511, 913, and 1090, with paleolatitudes between ~45° and 70° in both hemispheres (*18*), and sites 628, 803, 925, 929, 998, and 1218 in the tropics (Fig. 1 and table S1) (*19*). Chronologies for these sites were previously established or refined and/or determined in this study (table S2 and fig. S1). TEX_{86} indices were converted to SST by use of a modified temperature calibration based on all published ocean surface sediment data (fig. S2) (*20*). Nonetheless, older calibrations would yield qualitatively similar results over the temperature ranges observed.

Both $U^{K'}_{37}$ and TEX_{86} SSTs show substantial high-latitude cooling between ~34 and 33 Ma (Fig.

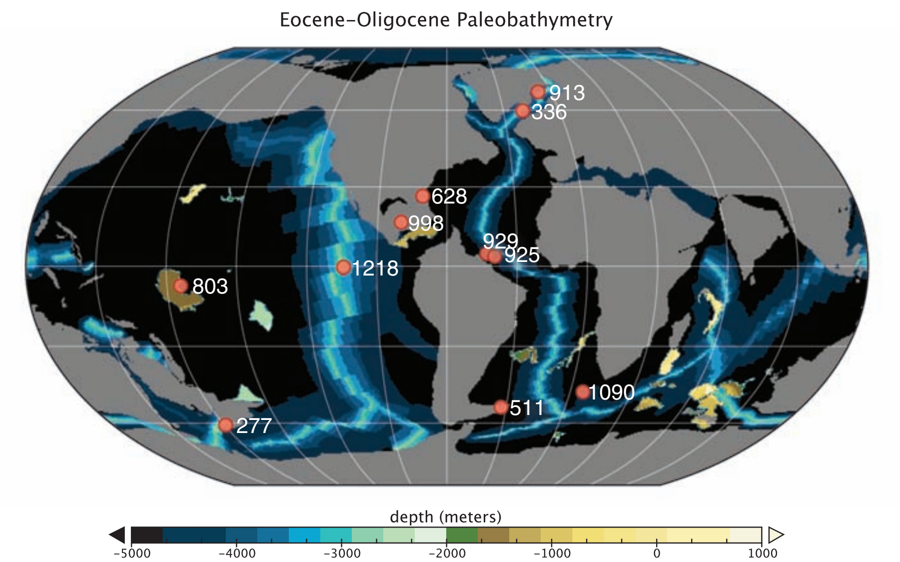

Fig. 1. Paleolocations of DSDP and ODP sites used in this study, superimposed on a map of reconstructed E-O bathymetry and geography (*18*).

[1]Department of Geology and Geophysics, Yale University, New Haven, CT 06520, USA. [2]Department of Earth Sciences, University of Hong Kong, Hong Kong, People's Republic of China. [3]Department of Geosciences, University of Massachusetts-Amherst, Amherst, MA 01003, USA. [4]Department of Earth and Atmospheric Sciences, Purdue University, West Lafayette, IN 47907, USA. [5]Laboratory of Palaeobotany and Palynology, Utrecht University, Budapestlaan 4, 3584 CD Utrecht, Netherlands. [6]Department of Earth and Planetary Sciences, Harvard University, Cambridge, MA 02138, USA.

*To whom correspondence should be addressed. E-mail: zhliu@hku.hk (Z.L.); mark.pagani@yale.edu (M.P.)